

## A THREE-DIMENSIONAL DEFLAGRATION MODEL FOR TYPE Ia SUPERNOVAE COMPARED WITH OBSERVATIONS

F. K. RÖPKE,<sup>1,2,3</sup> W. HILLEBRANDT,<sup>1,3</sup> W. SCHMIDT,<sup>4</sup> J. C. NIEMEYER,<sup>4</sup> S. I. BLINNIKOV,<sup>1,5</sup> AND P. A. MAZZALI<sup>1,3,6</sup>

*Received 2007 March 16; accepted 2007 July 3*

### ABSTRACT

A simulation of the thermonuclear explosion of a Chandrasekhar-mass C+O white dwarf, the most popular scenario of a Type Ia supernova (SN Ia), is presented. The underlying modeling is pursued in a self-consistent way, treating the combustion wave as a turbulent deflagration using well tested methods developed for laboratory combustion and based on the concept of “large-eddy simulations” (LESs). Such consistency requires to capture the onset of the turbulent cascade on resolved scales. This is achieved by computing the dynamical evolution on a  $1024^3$  moving grid, which resulted in the best-resolved three-dimensional SN Ia simulation carried out thus far, reaching the limits of what can be done on present supercomputers. Consequently, the model has no free parameters other than the initial conditions at the onset of the explosion, and therefore it has considerable predictive power. Our main objective is to determine to which extent such a simulation can account for the observations of normal SNe Ia. Guided by previous simulations with less resolution and a less sophisticated flame model, initial conditions were chosen that yield a reasonably strong explosion and a sufficient amount of radioactive nickel for a bright display. We show that observables are indeed matched to a reasonable degree. In particular, good agreement is found with the light curves of normal SNe Ia. Moreover, the model reproduces the general features of the abundance stratification as inferred from the analysis of spectra. This indicates that it captures the main features of the explosion mechanism of SNe Ia. However, we also show that even a seemingly best-choice pure deflagration model has shortcomings that indicate the need for a different mode of nuclear burning at late times, perhaps the transition to a detonation at low density.

*Subject headings:* hydrodynamics — instabilities — methods: numerical — supernovae: general — turbulence

### 1. INTRODUCTION

Understanding the physics of Type Ia supernova (SN Ia) explosions is a necessary premise for using them as cosmic distance indicators with confidence. Consequently, the development of three-dimensional explosion models has been a major challenge in astrophysics over the past decade. Only recently, however, has a self-consistent three-dimensional treatment of the turbulent thermonuclear flame in a white dwarf (WD) star avoiding free parameters become available. The ultimate goal of these efforts is to describe the full observational set of SNe Ia and even to predict their observed properties, such as their luminosities, light curves, and spectra, from first principles, with sufficient accuracy to guide the empirical calibration of their peak luminosity.

While this stage of sophistication has clearly not yet been reached with current simulations, at least one (perhaps in some cases the dominant) part of the mechanism can already be treated in a nonparameterized approach. In the first stage of the supernova explosion the flame propagates subsonically and is accelerated by turbulence, creating a problem of turbulent combustion physics. The knowledge on this subject acquired for laboratory combustion in engineering sciences can be transferred to astrophysics, facilitating self-consistent simulations with particular emphasis on the correct representation of the flame/turbulence

interaction (Niemeyer & Hillebrandt 1995; Reinecke et al. 1999a, 1999b, 2002a, 2002b; Röpke 2005, 2006b; Röpke & Hillebrandt 2005a; Schmidt & Niemeyer 2006; Schmidt et al. 2006b). In fact, most of the properties of turbulent chemical flames are recovered in SNe Ia, and the largely different relevant length scales, the simpler reaction kinetics, and the absence of complicated boundaries, make computations of thermonuclear supernovae perhaps easier than designing a new car engine, provided the initial conditions of the explosion are known.

Recent results from several three-dimensional simulations (Reinecke et al. 2002b; Gamezo et al. 2003; Travaglio et al. 2004; Röpke & Hillebrandt 2005a; Bravo & García-Senz 2006; Röpke et al. 2006b; Schmidt & Niemeyer 2006) indicate that a turbulent thermonuclear deflagration—a subsonic flame propagation—alone can lead to powerful explosions of WD stars. In combination with the elimination of free parameters in the model, the question arises as to what extent the results of such simulations match observational constraints. This question motivated several previous studies which addressed initial parameters of the exploding WD (Röpke & Hillebrandt 2004; Travaglio et al. 2005; Röpke et al. 2006a), the flame ignition configuration (Reinecke et al. 2002b; Röpke et al. 2006b; Schmidt & Niemeyer 2006), symmetry constraints in the simulation setup (Röpke & Hillebrandt 2005a), and the particular choice of the turbulence model (Schmidt et al. 2006b), as well as the impact of some initial conditions on observational results (Blinnikov et al. 2006).

One question left out until now, however, was whether the results would change significantly with higher resolution. The flame/turbulence interaction determines the propagation of the burning front and thus the results of the model with respect to nucleosynthesis and energetics. Given the expected strong turbulence effects and the associated vast range in relevant length scales, this endeavor may seem hopeless. However, as discussed below,

<sup>1</sup> Max-Planck-Institut für Astrophysik, Karl-Schwarzschild-Strasse 1, D-85741 Garching, Germany.

<sup>2</sup> Department of Astronomy and Astrophysics, University of California, Santa Cruz, 1156 High Street, Santa Cruz, CA 95064.

<sup>3</sup> Kavli Institute for Theoretical Physics, University of California, Santa Barbara, CA 93106.

<sup>4</sup> Lehrstuhl für Astronomie und Astrophysik, Universität Würzburg, Am Hubland, D-97074 Würzburg, Germany.

<sup>5</sup> SSC RF ITEP, Bolshaya Chermushkinskaya 25, 117218 Moscow, Russia.

<sup>6</sup> Istituto Nazionale di Astrofisica, OATs, via Tiepolo, 11, 34131 Trieste, Italy.

with the numerical modeling strategy pursued here, it turns out to be sufficient to resolve the onset of turbulence on the computational grid in order to recover a definitive result. The necessary resolution can be reached with current computational resources and marks the aim of the present study. A direct comparison with observational data is possible and is indeed pursued in this publication for one particular simulation in the framework of the pure deflagration model. With what is so far the best resolved three-dimensional simulation of the deflagration scenario for SNe Ia we assess its consistency and its compatibility with observations. As we show in this paper, such a state-of-the-art deflagration model matches observational data surprisingly well, although not all details are reproduced perfectly. As is argued below, the simulation reaches a state where the physical effects are resolved so that its predictions are expected to be robust and to reflect generic properties of the deflagration scenario.

Of course, a single simulation cannot provide the basis for general conclusions on the validity of the deflagration model. Here, we present a simulation performed within the range of realistic initial conditions (as far as they are known), but explicitly set up the initial flame configuration in a favorable way with regard to energy and  $^{56}\text{Ni}$  production. Combining this single realization of the deflagration model with the exploration of the parameter space carried out previously (and partially with simpler modeling approaches and less resolved simulations), successes and limitations of the deflagration model become visible and will be discussed accordingly (see § 7). In particular, some persisting shortcomings of the deflagration model can be taken as an indication that the deflagration stage alone cannot explain all aspects of SNe Ia. In some cases models beyond the deflagration regime are supported by observational results (e.g., Mazzali et al. 2007; Wang et al. 2007), but uncertain or even hypothetical physical mechanisms generally introduce free parameters into the models and make a face-to-face comparison with observations more difficult than in the case of the pure deflagration model.

## 2. ASTROPHYSICAL MODEL

Recent observations (e.g., Mazzali et al. 2007) support the scenario that the majority of SNe Ia originate from a carbon-oxygen WD disrupted by a thermonuclear explosion (Hoyle & Fowler 1960) when it approaches the Chandrasekhar-mass limit by mass accretion from a binary companion, which may perhaps be a nondegenerate star (Ruiz-Lapuente et al. [2004]; for alternative progenitor scenarios see, e.g., Hillebrandt & Niemeyer [2000]). Caused by temperature fluctuations inside the convective core of the electron-degenerate WD, small regions near its center are thought to commence a thermonuclear runaway with rapidly increasing nuclear energy release from burning the carbon-oxygen fuel to heavier elements. This process marks the birth of the thermonuclear flame. The exact number and distribution of ignition kernels is not well determined yet, implying that the largest uncertainty lies in the initial parameters of the explosion. The virtue of three-dimensional explosion models is that they directly relate the ignition conditions to the outcome of the explosion without introducing additional parameters. Thus, a comparison with observations sheds light on two aspects of the supernova problem: the progenitor evolution giving rise to these initial conditions and the explosion mechanism itself.

Here, we are concerned with the latter, for which several possibilities have been suggested. Hydrodynamically, two fundamentally distinct modes of flame propagation are admissible: a subsonic deflagration and a supersonic detonation. A prompt detonation would incinerate the entire star at the high initial densities, leading to conditions where nuclear reactions produce almost

exclusively iron group elements (Arnett et al. 1971). These are found to be abundant in the ejecta, predominantly produced as radioactive  $^{56}\text{Ni}$ . In its decay to  $^{56}\text{Co}$  (and later  $^{56}\text{Fe}$ ) gamma rays and positrons are emitted which downscatter to optical wavelengths in the SN ejecta and give rise to the observed optical display. At later times, in the so-called nebular spectra, this iron can be directly observed. However, failure to produce the intermediate-mass elements (e.g., silicon, calcium, and sulfur) observed with appreciable abundances in the early spectra of SNe Ia (for a review, see Filippenko 1997) rules out the prompt detonation mechanism. In contrast, a subsonic deflagration leaves enough time for the stellar material to expand before it is reached by the thermonuclear flame (Nomoto et al. 1976). Therefore, some burning takes place at densities low enough that mostly intermediate-mass elements are synthesized, while most  $^{56}\text{Ni}$  is produced during the early deflagration phase.

A laminar deflagration wave, mediated by microphysical heat transport, would propagate far too slowly to cause the WD to explode. However, as burning ignites near the WD's center and propagates outward, a stratification of low-density ashes below denser fuel emerges which is buoyancy-unstable in the gravitational field of the star. This configuration eventually leads to the formation of ascending burning bubbles. Their interfaces are subject to shear. Since typical Reynolds numbers of the flow are of the order of  $10^{14}$ , strong turbulent eddies must form which decay to smaller scales in a turbulent cascade. This has tremendous impact on the flame propagation. The flame surface is corrugated by turbulent velocity fluctuations, and its area increases dramatically, which enhances the burning rate. This acceleration of the flame speed and the fuel consumption rate enable explosions of the WD (e.g., Reinecke et al. 2002b).

The energy input into turbulent eddies is due to the Rayleigh-Taylor instability on the largest scales ( $\sim 100$  km). However, the flame interacts with turbulent velocity fluctuations down to much smaller scales. As demonstrated in § 5 below, these velocity fluctuations originate from an inertia-driven turbulent cascade. They do not obey a simple buoyancy-dominated scaling and therefore require special modeling effort.

## 3. NUMERICAL IMPLEMENTATION

Numerical schemes to model the propagation of a deflagration front in a SN Ia have been developed over the past years and have reached a high level of sophistication. The major challenge in the numerical implementation of the concept outlined in § 2 is posed by the vast range of relevant scales. It spans about 11 orders of magnitude, from the radius of the WD ( $\sim 2000$  km and expanding in the explosion) down to the Kolmogorov scale (less than a millimeter) where turbulent energy is dissipated. The flame interacts with turbulence down to the Gibson scale at which the laminar flame propagation speed becomes comparable to the turbulent velocity fluctuations. For most parts of the supernova explosion this scale is considerably larger than the flame width ( $\leq 1$  mm). Therefore, the interaction of the flame with turbulence is purely kinematic and burning takes place in the so-called flamelet regime of turbulent combustion (e.g., Peters 2000). Here, the flame propagation speed completely decouples from the microphysics of the burning and is entirely determined by turbulence effects. This also implies that the flame propagation does not scale with the laminar burning speed.

The challenge of scales can be tackled in an elegant way by employing a *large-eddy simulation* (LES) strategy. This approach resolves only the largest scales of the turbulent cascade and models the unresolved scales, so that it becomes possible to accommodate the entire WD on the computational domain. When seen

from the scale of the WD, the flame appears as a sharp discontinuity separating the fuel from the ashes. A suitable numerical scheme to track the propagation of such an interface is the level-set method (Osher & Sethian 1988; Smiljanovski et al. 1997; Reinecke et al. 1999b), where the flame front is associated with the zero level set of a signed distance function  $G$  set up to be negative in the fuel regions and positive in the ashes. The propagation velocity of this interface is given by the effective turbulent burning speed at the grid scale, which in the flamelet regime is completely determined by turbulent velocity fluctuations on that scale. These, in turn, are derived from a subgrid-scale turbulence model (for details, see Schmidt et al. 2006a, 2006b) which follows the properties of turbulence on unresolved scales based on filtering the velocity fluctuations on the resolved scales. This way, a localized treatment of the turbulent properties of the flow becomes feasible and the flame/turbulence interaction is modeled self-consistently.

The hydrodynamics is described by the reactive Euler equations (with gravity as an external force) and numerically—discretized on a Cartesian computational grid—treated in a finite-volume approach (Fryxell et al. 1989). Of course, the tremendous expansion of the WD during the explosion has to be taken into account. This was achieved by employing two nested moving grids: a fine uniform inner grid tracking the flame and a coarse outer grid capturing the WD (Röpke 2005; Röpke et al. 2006b).

With this implementation we performed what is thus far the largest simulation of a thermonuclear supernova explosion. It was set up on more than a billion computational grid cells (a  $1024^3$  cell grid). This allowed for a very fine resolution (down to  $\sim 870$  m) of the central part of the WD at the beginning of the explosion facilitating an exceptionally fine-structured initial flame configuration that was composed of 1600 spherical kernels of radius 2.6 km distributed inside a sphere extending 180 km around the center of the WD (see Fig. 1, *top left panel*). Although the details of the ignition process are yet unknown, analytical and numerical studies support such a multispot ignition configuration (e.g., Garcia-Senz & Woosley 1995; Woosley et al. 2004) and the flame ignition kernels are expected to be of the order of a kilometer in diameter (Iapichino et al. 2006). The configuration chosen here is certainly one that favors burning near the center and (as multispot ignition scenarios do in general; Röpke et al. 2006b) enhances the burning and energy release over that found in centrally or sparsely ignited scenarios.

The nuclear reactions were treated in the approximative approach outlined by Reinecke et al. (2002a). Only five species were taken into account: the fuel consisted of a mixture of carbon and oxygen in equal amounts by mass, intermediate-mass elements were represented by magnesium, and a mixture of  $^{56}\text{Ni}$  and alpha particles represented nuclear statistical equilibrium (NSE) material. Depending on the fuel density ahead of the flame,  $\rho_u$ , the material was converted to NSE (if  $\rho_u > 5.25 \times 10^7 \text{ g cm}^{-3}$ ), in which case the nickel/alpha-particle ratio was adjusted according to temperature and density, to intermediate-mass elements (if  $5.25 \times 10^7 \text{ g cm}^{-3} > \rho_u > 5.0 \times 10^5 \text{ g cm}^{-3}$ ), or left unburned (for lower fuel densities). The threshold for burning to intermediate-mass elements was chosen lower than in previous simulations. As argued by Schmidt (2007) the level-set description of the flame propagation may be extended beyond the onset of distributed burning at which turbulent eddies penetrate the internal structure (the “thin reaction zones regime”). This commences as soon as the flame width becomes larger than the Gibson scale, an effect that is expected to occur at fuel densities  $\sim 10^7 \text{ g cm}^{-3}$ . However, at densities below  $\sim 10^6 \text{ g cm}^{-3}$  nuclear reactions will be slow compared to the expansion timescales and, moreover, turbulence will interact with the burning zone inside the flame structure,

giving rise to the completely distributed (“broken reaction zones”) regime. Therefore, the burning description adopted here may be too optimistic at low densities and overpredict the total amount of intermediate-mass elements synthesized in the explosion. On the other hand, at the late stages, where low fuel densities are reached, the amplitude of turbulent velocity fluctuations decreases rapidly. Therefore, not much material is burned here, such that the fuel consumption at very low densities becomes insignificant and the potential error introduced by uncertainties is expected to be small.

#### 4. EVOLUTION OF THE EXPLOSION PHASE

The evolution of the explosion stage proceeds in agreement with the expectations outlined in § 1. After ignition in a multitude of only partially overlapping flame kernels (see upper left panel of Fig. 1), the ash region grows due to burning and starts floating toward the surface. The individual kernels deform from their initially spherical shape into “mushroom cap”-like structures—typical for the nonlinear stage of the Rayleigh-Taylor instability—and grow. This causes them to merge, so that a connected flame structure forms. This structure evolves dominated by buoyancy instability on large scales and driven by the turbulent cascade on smaller lengths. The continued development of substructure and the merger of features create a deflagration structure with a complex pattern (see top right panel of Fig. 1). Burning and flotation drive the flame toward the surface of the WD. The fuel density drops as the flame moves outwards and due to radial stratification and the overall expansion of the WD caused by the energy deposit from nuclear burning. Once the fuel density falls below the threshold for the production of intermediate-mass elements, nuclear burning ceases. This occurs first at the leading features of the flame and subsequently in more central flame regions. Finally, no burning takes place anymore. At this point the outer ash features have reached the surface layers of the ejecta (bottom left panel of Fig. 1). The following seconds in the evolution are characterized by the hydrodynamical relaxation toward homologous expansion. This stage is reached to good approximation at about 10 s after ignition (Röpke 2005).

This three-dimensional evolution leads to a remnant of the explosion with characteristic properties. The density structure has patterns from unstable and turbulent flame propagation imprinted on it (see bottom right panel of Fig. 1) and ash regions extend to the outermost layers of the expanding cloud of gas.

The chemical composition of the ejecta of the explosion as followed in the hydrodynamical simulation is shown in Figure 2. The outer parts consist mainly of unburned carbon and oxygen, but some “bubbles” of intermediate-mass elements are also present near the surface (Fig. 2, *left*). The central part of the ejecta is dominated by iron group elements (Fig. 2, *right*). Inside the ash bubbles some mixing of different species is found, but still regions dominated by either iron group elements or intermediate-mass elements can be identified. The large-scale bubbles of ash are separated by a few thin but dense fingers of unburned material, so that the spherically averaged composition of the ejecta appears strongly mixed.

#### 5. CONSISTENCY OF THE SUBGRID-SCALE MODELING

The subgrid-scale model employed in the simulation couples the dynamics at unresolved scales to the numerically computed flow. The model is based on the balance equation for the subgrid-scale turbulent energy, where the energy production rate follows from a similarity assumption linking the smallest resolved to the largest unresolved scales (Schmidt et al. 2006a). Although the calculation of the rate of turbulence energy production is localized

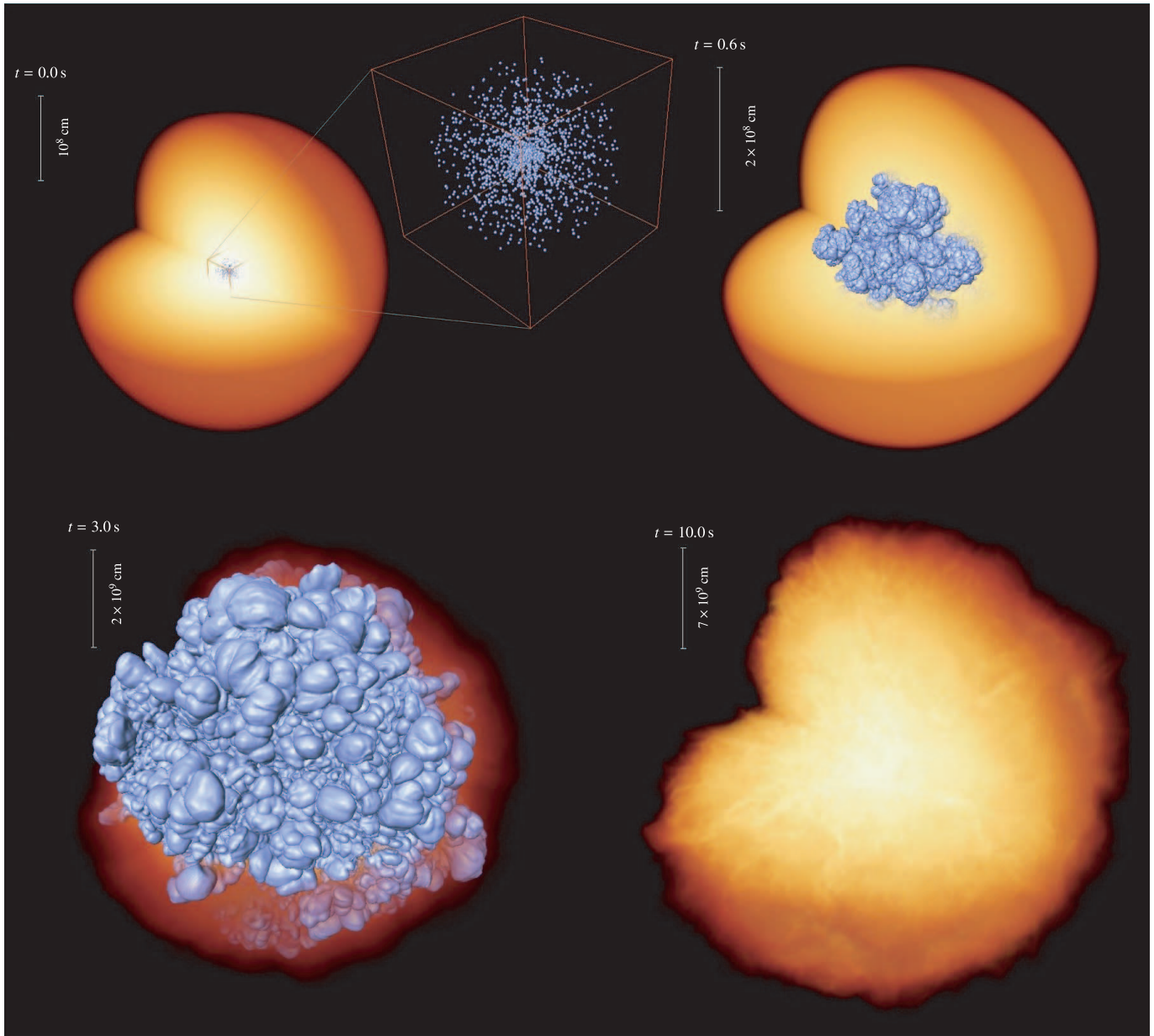


FIG. 1.— Evolution of the thermonuclear supernova explosion simulation. The zero level set associated with the thermonuclear flame is shown as a blue isosurface and the extent of the WD is indicated by the volume rendering of the density. The top left panel shows the initial setup, and the close-up illustrates the chosen flame ignition configuration. The subsequent two panels illustrate the propagation of the turbulent flame through the WD and the density structure of the remnant is shown in the bottom right panel.

and, consequently, does not rely on stationarity or large-scale homogeneity, asymptotic isotropy toward smaller length scales is required for consistency. In the case of incompressible turbulence, asymptotic isotropy becomes manifest in the Kolmogorov  $k^{-5/3}$  scaling for sufficiently large wavenumbers  $k$ . This scaling has been found in simulations of Rayleigh-Taylor unstable stratifications (Cabot & Cook 2006), as well as in buoyancy unstable flames in degenerate WD matter Zingale et al. (2005).

Figure 3 shows compensated energy spectrum functions,  $k^{5/3}E(k)$ , derived from our simulation for several instants of time ranging from 0.5 to 1.0 s after ignition. For turbulent velocity fields obeying Kolmogorov scaling, the compensated spectrum functions are expected to be constant. Wavenumbers are normalized by  $\pi/(512\Delta_0)$ , where  $\Delta_0$  is the cell size in the uniform part of the grid. Since the grid is inhomogeneous and does not satisfy periodic boundary conditions, the velocity fields obtained from the simulation were zero-padded in the outer regions with Gaussian

windowing functions in order to compute Fourier transforms. This is why the compensated spectrum functions are plotted for normalized wavenumbers greater than 16 only. At all times considered here, it can be seen that the spectrum functions are well approximated by the Kolmogorov power law for intermediate wavenumbers, thus indicating the presence of an inertial subrange. Therefore, the simulation is as well resolved as the modeling approach requires. Higher resolution is not expected to change the characteristics of the turbulent flame propagation.

## 6. RESULTS AND COMPARISON WITH OBSERVATIONS

The present deflagration simulation of a thermonuclear supernova makes distinct predictions for observables that can be tested against real SNe Ia. With certain observables like polarimetry spectra and spectra of the nebular phase it may be possible to check details of the results of pure deflagration models against observations and potentially assess its validity. This certainly

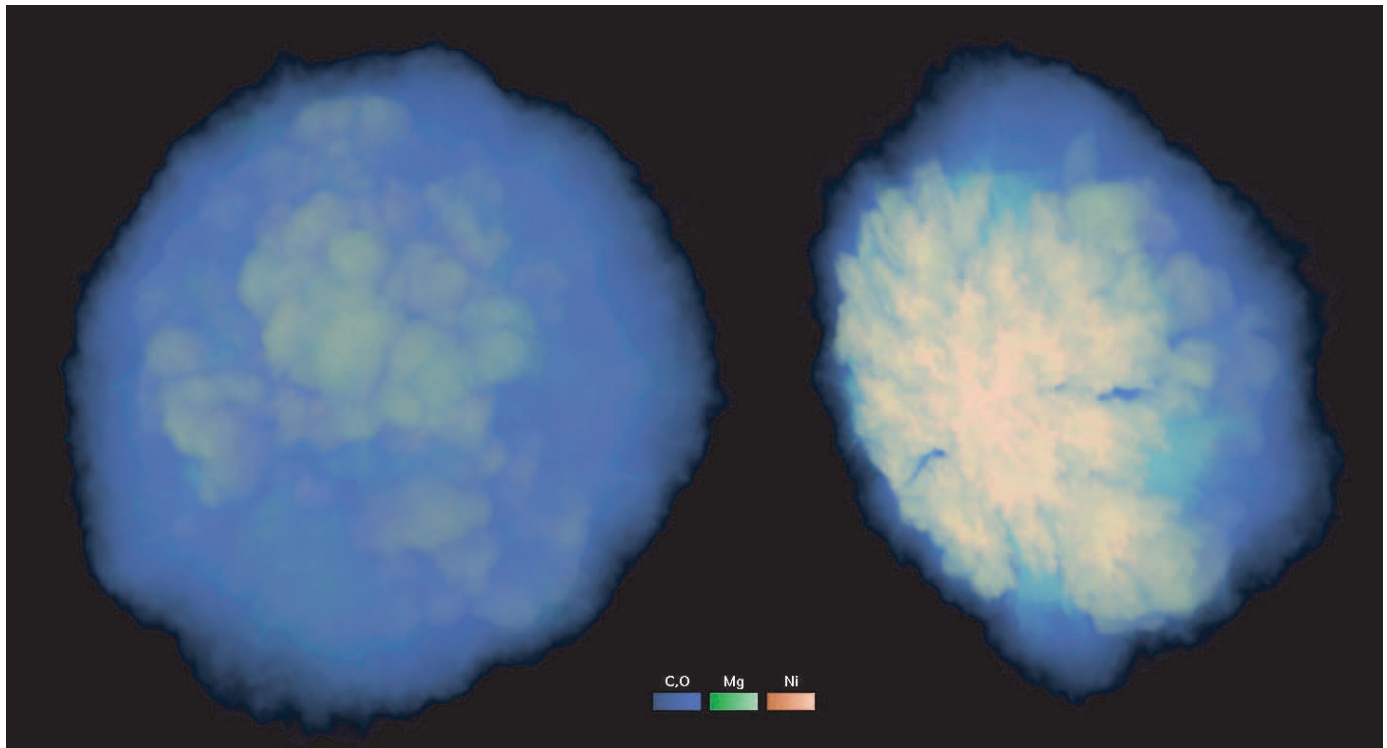


FIG. 2.— Composition of the remnant after the explosion ( $t = 10$  s). The products of the mass fractions of three of the species followed in the hydrodynamical explosion simulation with density are volume rendered in different colors. The right panel shows a cutaway to illustrate the composition of the central parts.

warrants further attention and will be addressed in future work. Here, we are concerned with some more basic global properties which test whether our particular simulation falls into the range of observations.

The asymptotic kinetic energy amounted to  $8.1 \times 10^{50}$  erg. In the hydrodynamical simulation,  $0.606 M_{\odot}$  of iron group elements and  $0.431 M_{\odot}$  of intermediate-mass elements were produced, leaving behind  $0.368 M_{\odot}$  of unburned carbon and oxygen.

The composition of the ejecta can be directly compared with that of observed supernovae obtained from abundance tomography (Stehle et al. 2005) using a spherical average over the entire ejecta of the model in homologous expansion. Such a comparison with the abundance tomography of SN 2002bo is shown in Figure 4, where the velocity is used as radial coordinate. Two cau-

tionary remarks are necessary here. First, SN 2002bo was a much more energetic and luminous event than that expected to result from the simulation. Second, as pointed out in § 4, there exist features with high concentrations of particular species (see Fig. 2) large enough to dominate spectral observations. The procedure of spherically averaging the mass fractions washes out these structures and artificially increases the mixing of species. Nonetheless, the chemical composition of the ejecta of the simulated explosion and the abundance tomography of SN 2002bo compare surprisingly well. In both cases, the central parts are clearly dominated by

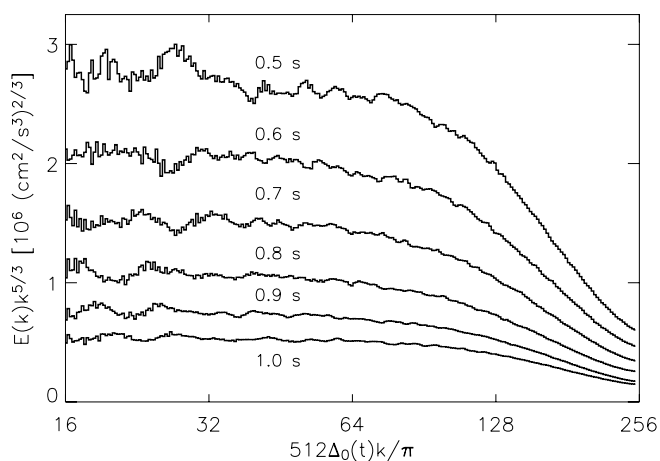


FIG. 3.— Compensated energy spectrum functions derived from our simulation at different instants in time.

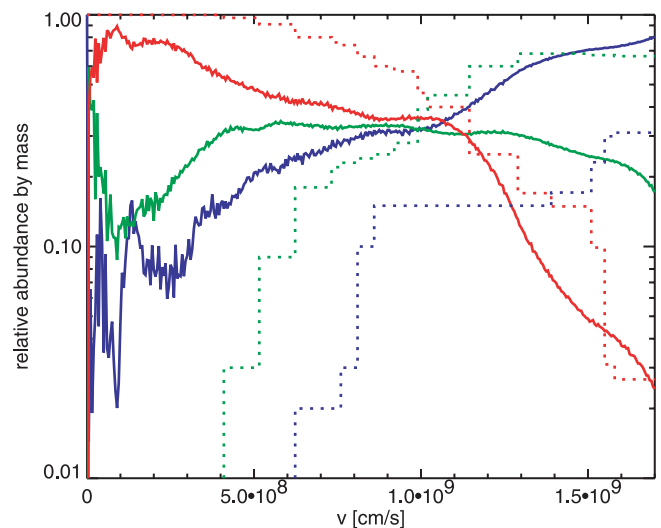


FIG. 4.— Spherically averaged composition resulting from the hydrodynamical explosion simulation (solid lines) compared to the findings of the abundance tomography of SN 2002bo (dotted lines). Iron group element abundances are shown in red, intermediate-mass elements in green, and unburned material in blue.

iron group elements and the overall distribution of the main species in our simulation generally agrees with that obtained from the abundance tomography. There is good agreement up to velocities of  $\sim 10,000 \text{ km s}^{-1}$ , if we keep in mind that SN 2002bo had a  $^{56}\text{Ni}$  content of  $\sim 0.5 M_{\odot}$ , which is significantly larger than in the simulation. The slope of the decline of the iron group abundance toward larger radii is also well reproduced. These elements are mixed out to the same radii in the simulation and in the observation. Moreover, both agree in intermediate-mass elements being more abundant than unburned material below  $\sim 10,000 \text{ km s}^{-1}$  and mixed compositions over a wide range of velocities. The abundance of unburned material in the simulation is low in this velocity range, in particular near the center. As previously pointed out by Kozma et al. (2005), the presence of large amounts of unburned fuel at low velocities gives rise to a pronounced oxygen line in the late-time (“nebular”) spectra which is inconsistent with observations. Owing to the more complete burning of the center with the chosen flame ignition condition, this problem is alleviated in the current simulation. The abundance of fuel material near the center is lower by a factor of 10–50 than the iron group mass fraction here.

Still, the abundance of carbon and oxygen seems rather high in comparison with the observation. This may in part be an artifact of the spherical averaging procedure for determining the composition of the ejecta in the simulation. Overestimating the contribution of the dense but narrow fuel regions (see Fig. 2). As the volume of ejecta that influences the spectra taken from a certain line of sight varies with time, a careful analysis of this effect would require the derivation of spectra from our simulation in a three-dimensional approach.

At velocities above  $\sim 10,000 \text{ km s}^{-1}$ , however, there is a significant discrepancy between the abundance tomography data of SN 2002bo and the simulated composition. While in the former the intermediate-mass elements dominate out to high velocities, the ejecta in the simulation quickly become dominated by unburned material. This discrepancy, however, is only found in the outer  $0.25 M_{\odot}$ .

In order to derive light curves from the simulation, more detailed information about the chemical composition of the ejecta is necessary than the data obtained directly from the hydrodynamical explosion simulation. This information can be derived in a nucleosynthetic postprocessing step (Travaglio et al. 2004) on the basis of  $53^3$  tracer particles that have been advected in the flow. The mass of the star was equally distributed between those tracers, and they add a “Lagrangian component” to the otherwise Eulerian approach. Recording representative temperature and density profiles, they facilitate the a posteriori reconstruction of the nuclear reactions with a large reaction network (which would be impractical to employ concurrently with the explosion simulation). This way, the chemical composition of the ejecta as needed for the radiative transfer is determined. In particular, it is necessary to separate the  $^{56}\text{Ni}$ , which by radioactive decay provides the energy for the optical event, from the stable iron group isotopes that do not contribute to the luminosity but are important for absorption. The postprocessing yields  $0.56 M_{\odot}$  of iron group elements ( $0.05 M_{\odot}$  less than the estimate from the hydrodynamical simulation) and  $0.33 M_{\odot}$  of  $^{56}\text{Ni}$ . This indicates that the simulated supernova would range among the lower end of observed normal SNe Ia. For events like SN 1991M, SN 1993L, SN 2004eo, and SN 2001el similar masses of  $^{56}\text{Ni}$  and total iron group elements were inferred by Mazzali et al. (2007).

On the basis of the ejecta composition as derived from the postprocessing step and spherically averaged over the entire star, bolometric light curves (true bolometric as well as “UVOIR-bolometric”) have been derived with the radiative transport code STELLA, as

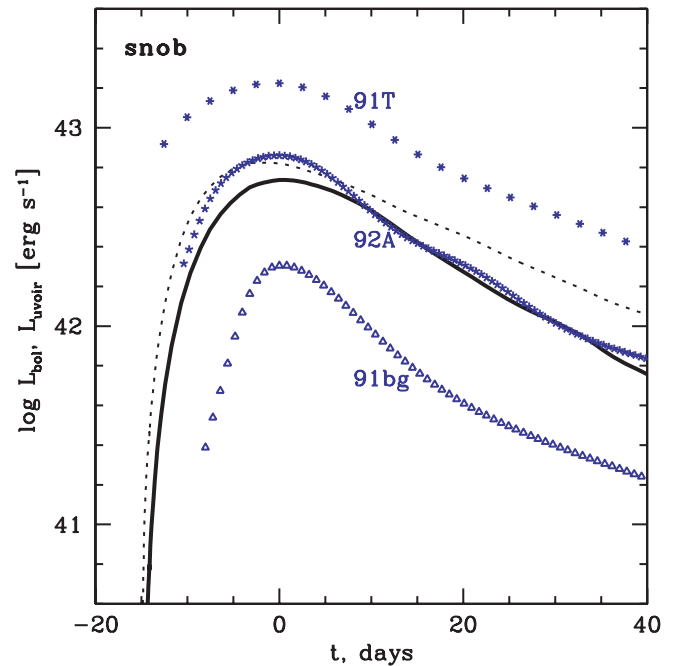


Fig. 5.— Bolometric light curve derived for our model (black curves; solid line is the “UVOIR-bolometric” light curve and the complete bolometric light curve is a dotted line). The blue dotted curves correspond to observed bolometric light curves (Stritzinger et al. 2006).

described in detail by Blinnikov et al. (2006). The result is shown in Figure 5 and compared to the bolometric light curves of standard SNe Ia as given by Stritzinger et al. (2006). Evidently, the synthetic light curve derived from the simulation is a normal SN Ia light curve both in terms of the peak luminosity and the shape. It is slightly dimmer than SN 1992A, as expected from the lower  $^{56}\text{Ni}$  mass (Stritzinger et al. [2006] report  $0.4 M_{\odot}$  of  $^{56}\text{Ni}$  for SN 1992A), but has a very similar rise and decline rate.

## 7. LIMITS OF THE PURE DEFLAGRATION MODEL

The limited success of the presented simulation in reproducing the observables of SNe Ia raises the question of whether it is possible to assess generic limits of the pure deflagration model on this basis. Since a realization in a single simulation does not cover the full parameter space, this has to be discussed in combination with simulations performed previously. Reinecke et al. (2002b), Röpke & Hillebrandt (2004), Travaglio et al. (2005), Röpke et al. (2006a, 2006b), and Schmidt & Niemeyer (2006) explored the impact of various initial conditions on the explosion process. These simulations were not performed with the same resolution as the one presented here and are partially based on the simpler subgrid-scale turbulence model proposed by Niemeyer & Hillebrandt (1995). Still these results can guide an assessment of the deflagration model, since the changes between the two subgrid-scale models are moderate (at most 30% in the iron group element production and the energy release; Schmidt et al. 2006b).

The two main shortcomings identified in § 6 were (1) the overall low explosion strength resulting in a low  $^{56}\text{Ni}$  production and a low explosion energy and (2) the underproduction of intermediate-mass elements in the outer layers of the ejecta. Problem 1 has been noted in all deflagration simulations based on a consistent approach of modeling the flame propagation. There are, however, several initial parameters that may remedy the problem. These have been tested in previous simulations.

Clearly, a major parameter is the geometrical configuration of the flame ignition. With simple central ignitions (“C3” setups of Reinecke et al. [2002b]; Röpke & Hillebrandt [2005a]), the asymptotic kinetic energy of the ejecta falls around  $4.5 \times 10^{50}$  erg and the masses of produced iron group elements hardly exceed  $0.5 M_{\odot}$ , with  $\sim 0.3 M_{\odot}$  of it being  $^{56}\text{Ni}$ . This would account for the dimmest examples among the “normal” SNe Ia. Ignition in multiple spots around the center evidently increases the explosion strength. For a model ignited in 30 bubbles per octant, Travaglio et al. (2004) report an asymptotic kinetic energy of about  $6.5 \times 10^{50}$  erg and a  $^{56}\text{Ni}$  production of  $0.418 M_{\odot}$ . Röpke et al. (2006b) explored the impact of multispot ignitions in a systematic approach and found an optimum of such configurations resulting in an asymptotic kinetic energy of  $6.8 \times 10^{50}$  erg and  $0.67 M_{\odot}$  of iron group elements. The latter value may increase in modeling the ignition as a stochastic process in time to  $\sim 0.75 M_{\odot}$  (Schmidt & Niemeyer 2006). Given these values, the choice of the ignition configuration in the present model was moderately optimistic, producing  $0.606 M_{\odot}$  of iron group elements, about  $0.33 M_{\odot}$  of which is  $^{56}\text{Ni}$ . A large ratio of produced stable-to-radioactive iron group elements (here it amounts to 0.59) seems to be a general feature of turbulent deflagration models ignited in a multitude of ignition kernels, since most of the iron group synthesis proceeds here at the early stages, where high densities prevail such that electron capture reactions are significant.

Other parameters that have an impact on the  $^{56}\text{Ni}$  production and the energy release are the central density of the WD at ignition and its metallicity. A higher central density naturally increases the amount of material available that potentially can burn to iron group elements. Moreover, the increased gravitational acceleration will enhance the buoyancy-induced turbulence and accelerate the flame. On the other hand, with increased densities electron captures become more important and will favor the production of stable iron group isotopes over  $^{56}\text{Ni}$ . The effect of varying the central density has been addressed by Röpke et al. (2006a). In a density range where electron captures are still moderate, increasing the central density by a factor of 2.6 changes the  $^{56}\text{Ni}$  yield only by less than 10%, although the total iron group element synthesis was enhanced by  $\sim 30\%$ . Therefore, although energetic results and enhanced production of the iron group are expected with higher central densities of the exploding WD star, as electron capture reactions become important the fraction of  $^{56}\text{Ni}$  in the NSE material and thus the brightness of the corresponding events will decrease. An overproduction of stable iron group nuclei is anticipated here. Turning this argument around, a way to obtain higher  $^{56}\text{Ni}$  masses (although the total mass of iron group and intermediate-mass elements would not increase) would be to consider a WD with lower central density ignited in a multispot scenario. This issue will be addressed in a forthcoming study, but as the results of Röpke et al. (2006a) indicate, the effect is not expected to be sufficient to account for the brighter observed SN Ia events.

The metallicity of the WD material will have little effect on the iron group production and the energy release, but evidently affects the ratio of stable to radioactive iron group element masses. Increasing the metallicity favors the production of neutron-rich stable nuclei over  $^{56}\text{Ni}$  (Timmes et al. 2003; Travaglio et al. 2005; Röpke et al. 2006b) and makes the corresponding event dimmer. The  $^{56}\text{Ni}$  masses decrease linearly with metallicity, and the values given above were derived under the assumption of solar metallicity. Thus, metallicity effects have no potential of increasing the  $^{56}\text{Ni}$  yields of the deflagration model significantly.

Issue 2 is equivalent with the incomplete burning of the outer layers of the WD star. Here, the problem of modeling the flame

propagation at conditions where the flamelet picture breaks down becomes important. It has been shown that a flame acceleration in this phase would significantly enhance the production of intermediate-mass elements and the energy release (Röpke & Hillebrandt 2005b), but Schmidt (2007) argues that such an acceleration does not occur and that a continuation of modeling the flame propagation as in the flamelet regime is possible. This approach was followed here, too. Therefore, within the pure turbulent deflagration regime, it seems unrealistic to enhance burning at low densities beyond what was achieved in the current simulation.

We thus conclude that the initial parameters of the model are unlikely to leave enough room to adjust the simulations in order to account for the more powerful SN Ia events and to reproduce the chemical composition in the outer layers of the ejecta. As the model of flame propagation itself leaves no free parameters, only such initial parameters of the WD and the flame ignition come into consideration here. These have been tested, and adjusting the simulations in a favorable way allows them to enter the range of the weaker “normal” SNe Ia in terms of  $^{56}\text{Ni}$  production, explosion energy, and composition of the inner part of the ejecta. The more powerful observed events, producing close to  $1 M_{\odot}$  of  $^{56}\text{Ni}$  (e.g., Mazzali et al. 2007) are clearly out of reach for the pure deflagration scenario of SNe Ia.

## 8. CONCLUSIONS

We presented a three-dimensional deflagration simulation of a thermonuclear supernova explosion with the astrophysical modeling and numerical implementation designed in a way to allow for self-consistent simulation. The model contains no tunable parameters except for the flame ignition condition, which is physically not well determined yet, and the initial conditions of the WD, which may vary from event to event in nature. An additional uncertainty of the model is due to burning at the lowest fuel densities, which needs further attention, but is expected to lead to only minor changes in the conclusions about the gross properties of the simulation which we present here. Clearly, the most significant parameter is the flame ignition configuration, which even decides the success of the deflagration burning in causing the white dwarf star to explode (e.g., Calder et al. 2004; Plewa et al. 2004; Röpke et al. 2007). Here, it was set up in a favorable way in order to burn the fuel material at the center of the star as completely as possible and to maximize the energy and  $^{56}\text{Ni}$  production.

The goal of the simulation was to reach a regime in which the flame/turbulence interaction modeling is fully self-consistent, which requires us to resolve the onset of the turbulent cascade on the computational grid. This was achieved by performing the simulation with unprecedented resolution. Such a consistent implementation of the burning model allows the direct confrontation with observables. The comparison with bolometric light curves and the chemical composition of the ejecta derived from observed spectra showed that the simulated explosion indeed reproduces the characteristics of the observed fainter examples of normal SNe Ia. Gross properties of the simulations, such as energy the energy release and the  $^{56}\text{Ni}$  production were also consistent with expectations from SN Ia observations. One has to note, however, that even choosing favorable ignition conditions (a slight improvement is possible with a time-dependent stochastic distribution of ignition kernels; Schmidt & Niemeyer 2006), the explosion energy and the brightness of the model event fall toward the lowest values observed for normal SNe Ia.

Thus, on comparison with previous results from lower resolved simulations exploring the range of the initial parameters, we conclude that within the astrophysical model employed here, it seems impossible to reproduce the more energetic events of

the observed SN Ia sample. Also, a smooth shell of intermediate-mass elements surrounding the iron-rich core of the ejecta cloud and the anticorrelation between the iron-group and the intermediate-mass elements in the ejecta (Mazzali et al. 2007) are difficult to explain within this framework. Therefore, an extension of the scenario seems necessary. The shortcomings of the model in reproducing the chemical composition of the ejecta in the outer parts while providing good agreement with the observations in central regions may be taken as an indication that the deflagration phase is only the first phase of the explosion mechanism. While the reasonable agreement with observables of weaker SN Ia events indicates that it may be the dominant part of the explosion mechanism here, the discrepancy is obvious for the brighter parts of the SN Ia sample. Possible extensions of the model include an improved description of burning in the distributed burning regime at low fuel densities, as well as a transition to a supersonic detonation mode of flame propagation at the onset of this regime. Recently, Röpke & Niemeyer (2007) modeled delayed detonation scenarios in three dimensions under the assumption that the deflagration-to-detonation transition occurs as the flame enters the distributed burning regime. Depending on the configuration of the deflagration flame ignition, a wide range of  $^{56}\text{Ni}$  masses was recovered which would reproduce observations of normal to bright SNe Ia. In this context, the fainter examples correspond to events with a

pronounced deflagration phase. For these, most of the energy and  $^{56}\text{Ni}$  production originates from that phase and the character of the events is similar to pure deflagration models. Thus, our results may be interpreted as an indication that the fainter subsample of normal SNe Ia expose the hallmark of the deflagration phase. Since the strength of deflagration phase determined the overall characteristics of the delayed detonation model implemented this way, a careful and self-consistent treatment of the burning physics in the deflagration phases is a premise for credible modeling here as well.

The simulation presented here was carried out at the Computer Center of the Max Planck Society, Garching, Germany. The authors gratefully acknowledge the hospitality and the inspiring atmosphere at the Kavli Institute for Theoretical Physics at the University of California, Santa Barbara, where the paper was written. This work was supported by the European Research Training Network “The Physics of Type Ia Supernovae” under contract HPRN-CT-2002-00303 and the Deutsche Forschungsgemeinschaft via the Transregional Collaborative Research Centre TRR 33 “The Dark Universe.” F. K. R. received support from the NASA Theory Program (NNG05GG08G) and from the SciDAC program of the DOE (DE-FC02-01ER41176).

## REFERENCES

- Arnett, W. D., Truran, J. W., & Woosley, S. E. 1971, *ApJ*, 165, 87  
 Blinnikov, S. I., Röpke, F. K., Sorokina, E. I., Gieseler, M., Reinecke, M., Travaglio, C., Hillebrandt, W., & Stritzinger, M. 2006, *A&A*, 453, 229  
 Bravo, E., & García-Senz, D. 2006, *ApJ*, 642, L157  
 Cabot, W. H., & Cook, A. W. 2006, *Nature Phys.*, 2, 562  
 Calder, A. C., Plewa, T., Vladimirova, N., Lamb, D. Q., & Truran, J. W. 2004, preprint (astro-ph/0405162)  
 Filippenko, A. V. 1997, *ARA&A*, 35, 309  
 Fryxell, B. A., Müller, E., & Arnett, W. D. 1989, *Hydrodynamics and Nuclear Burning* (MPA Green Report 449; Garching: MPA)  
 Gamezo, V. N., Khokhlov, A. M., Oran, E. S., Chtchelkanova, A. Y., & Rosenberg, R. O. 2003, *Science*, 299, 77  
 García-Senz, D., & Woosley, S. E. 1995, *ApJ*, 454, 895  
 Hillebrandt, W., & Niemeyer, J. C. 2000, *ARA&A*, 38, 191  
 Hoyle, F., & Fowler, W. A. 1960, *ApJ*, 132, 565  
 Iapichino, L., Brügggen, M., Hillebrandt, W., & Niemeyer, J. C. 2006, *A&A*, 450, 655  
 Kozma, C., Fransson, C., Hillebrandt, W., Travaglio, C., Sollerman, J., Reinecke, M., Röpke, F. K., & Spyromilio, J. 2005, *A&A*, 437, 983  
 Mazzali, P. A., Röpke, F. K., Benetti, S., & Hillebrandt, W. 2007, *Science*, 315, 825  
 Niemeyer, J. C., & Hillebrandt, W. 1995, *ApJ*, 452, 769  
 Nomoto, K., Sugimoto, D., & Neo, S. 1976, *Ap&SS*, 39, L37  
 Osher, S., & Sethian, J. A. 1988, *J. Comput. Phys.*, 79, 12  
 Peters, N. 2000, *Turbulent Combustion* (Cambridge: Cambridge Univ. Press)  
 Plewa, T., Calder, A. C., & Lamb, D. Q. 2004, *ApJ*, 612, L37  
 Reinecke, M., Hillebrandt, W., & Niemeyer, J. C. 1999a, *A&A*, 347, 739  
 ———. 2002a, *A&A*, 386, 936  
 ———. 2002b, *A&A*, 391, 1167  
 Reinecke, M., Hillebrandt, W., Niemeyer, J. C., Klein, R., & Gröbl, A. 1999b, *A&A*, 347, 724  
 Röpke, F. K. 2005, *A&A*, 432, 969  
 Röpke, F. K., Gieseler, M., Reinecke, M., Travaglio, C., & Hillebrandt, W. 2006a, *A&A*, 453, 203  
 Röpke, F. K., & Hillebrandt, W. 2004, *A&A*, 420, L1  
 ———. 2005a, *A&A*, 431, 635  
 ———. 2005b, *A&A*, 429, L29  
 Röpke, F. K., Hillebrandt, W., Niemeyer, J. C., & Woosley, S. E. 2006b, *A&A*, 448, 1  
 Röpke, F. K., & Niemeyer, J. C. 2007, *A&A*, 464, 683  
 Röpke, F. K., Woosley, S. E., & Hillebrandt, W. 2007, *ApJ*, 660, 1344  
 Ruiz-Lapuente, P., et al. 2004, *Nature*, 431, 1069  
 Schmidt, W. 2007, *A&A*, 465, 263  
 Schmidt, W., & Niemeyer, J. C. 2006, *A&A*, 446, 627  
 Schmidt, W., Niemeyer, J. C., & Hillebrandt, W. 2006a, *A&A*, 450, 265  
 Schmidt, W., Niemeyer, J. C., Hillebrandt, W., & Röpke, F. K. 2006b, *A&A*, 450, 283  
 Smiljanovski, V., Moser, V., & Klein, R. 1997, *Combustion Theory and Modelling*, 1, 183  
 Stehle, M., Mazzali, P. A., Benetti, S., & Hillebrandt, W. 2005, *MNRAS*, 360, 1231  
 Stritzinger, M., Leibundgut, B., Walch, S., & Contardo, G. 2006, *A&A*, 450, 241  
 Timmes, F. X., Brown, E. F., & Truran, J. W. 2003, *ApJ*, 590, L83  
 Travaglio, C., Hillebrandt, W., & Reinecke, M. 2005, *A&A*, 443, 1007  
 Travaglio, C., Hillebrandt, W., Reinecke, M., & Thielemann, F.-K. 2004, *A&A*, 425, 1029  
 Wang, L., Baade, D., & Patat, F. 2007, *Science*, 315, 212  
 Woosley, S. E., Wunsch, S., & Kuhlen, M. 2004, *ApJ*, 607, 921  
 Zingale, M., Woosley, S. E., Rendleman, C. A., Day, M. S., & Bell, J. B. 2005, *ApJ*, 632, 1021